JMEPEG (2013) 22:1776–1782
DOI: 10.1007/s11665-012-0444-4

1059-9495/$19.00

Microstructure, Mechanical Properties, and Pyroconductivity of $NiFe_2O_4$ Composite Reinforced with ZrO_2 Fibers

Jinjing Du, Yihan Liu, Guangchun Yao, Zhongsheng Hua, Xiuli Long, and Bin Wang

(Submitted May 25, 2012; in revised form October 31, 2012; published online December 7, 2012)

NiO-Fe_2O_3-ZrO_{2f} composites were fabricated by a two-step sintering process. No phase transformation for ZrO_{2f} was observed. The as-prepared NiO-Fe_2O_3-ZrO_{2f} ceramic showed excellent mechanical properties because of the introduction of ZrO_2 fiber. The values for both the bending strength and fracture strength of 3 wt.% ZrO_{2f}-reinforced $NiFe_2O_4$ samples reached the maximum values of ~89.0 MPa and ~4.67 MPa $m^{1/2}$, respectively, The toughness mechanism is mainly attributed to fibers' fracture, crack deflection, fibers' pull-out, and fibers' debonding. The conductivity of ZrO_{2f}-reinforced $NiFe_2O_4$ is dependent on temperature and ZrO_{2f} content. When the electrolytic temperature is up to 950 °C, the conductivity value of the sample reinforced with 4 wt.% ZrO_2 fibers is 0.63 S/cm, which has been improved by 37.8% compared with the conductivity value of 0.45 S/cm for the un-doped samples. The main conductive mechanisms of ZrO_2 fiber in the matrix are the one based on the substitution of Zr^{4+} ions to produce quasi-free electrons, and the other based on oxygen ionic conducting mechanism.

Keywords ceramic matrix composites, conductivity, heat treating, mechanical testing, ZrO_2 fiber

1. Introduction

Nickel ferrite ($NiFe_2O_4$) is one of the most important spinel ferrites as well as a typical spin soft-magnetic ferrite (Ref 1). Its cubic inverse spinel structure shows ferromagnetism, which originates from magnetic moment of anti-parallel spins between Fe^{3+} ions at tetrahedral sites and Ni^{2+} ions at octahedral sites (Ref 2, 3). $NiFe_2O_4$ composites, as semiconductor-natured polycrystalline spinel ferrites, are applicable in many magnetic devices because of their low electrical conductivity values compared to those of magnetic materials (Ref 4-7). Because of its high initial electrical resistivity at ambient temperatures, $NiFe_2O_4$ composite was seldom employed to serve as electrode material (Ref 8). However, the cubic inverse spinel structure provides better chemical stability in the molten cryolite-alumina bath (Ref 9). Hence, it is possible for nickel ferrite ($NiFe_2O_4$) to be used as a promising candidate for green inert anodes at high temperatures. In order to examine this possibility, many efforts have been made to study the $NiFe_2O_4$ composites working as inert anodes, and some progress has been achieved (Ref 9-12). It is a proven fact that it can produce environment-friendly O_2 gas during electrolysis instead of greenhouse gases and fluorocarbons (Ref 12). Unfortunately, unsatisfactory fracture toughness and thermal shock resistance are still the obstacles preventing $NiFe_2O_4$ composite ceramics from being widely used, especially for applications in thermal shock conditions with high transfer and/or rapid environmental temperature changes, such as those experienced in electrolytic bath (Ref 13). One method for improving thermal shock resistance is to tailor the structure on multiple length scales to produce architectures that are engineered to enhance thermal shock resistance and improve fracture toughness while maintaining load-bearing capability. Another feasible method is to introduce a toughening phase, such as particles, whiskers, and fibers, into the ceramic matrix. It was recognized that fiber with certain aspect ratio is a promising candidate due to the complex toughening mechanisms (Ref 14). Since the discovery of the transformation toughening in ZrO_2 (Ref 15), a considerable effort has been performed to understand the microstructure and mechanical properties of ZrO_2-based ceramics. ZrO_2 is of particular interest as it undergoes at least three crystallographic transformations (monoclinic, tetragonal, and cubic) when it cools from high temperature to room temperature (Ref 16).

It has been shown that the ceramics reinforced by continuous fibers have promising potential for high-temperature application, especially for the ceramics reinforced by Y_2O_3-stabilized ZrO_2 fibers. It is due to the remarkable fracture toughening characteristic of the Y_2O_3-stabilized ZrO_{2f} through three mechanisms: fiber bridging, fiber pullout, and crack deflection (Ref 17-19). It was expected that the toughness can further be improved when both fiber toughening and phase transformation are incorporated into the ceramic matrix. Nevertheless, there are few reports about ZrO_2 fiber-toughened $NiFe_2O_4$ composites with respect to the cooperative toughening.

Jinjing Du and **Bin Wang**, School of Metallurgy Engineering, Xi'an University of Architecture and Technology, Box 208, Xi'an 710055, China and School of Materials and Metallurgy, Northeastern University, Box 117, Shenyang 110004, China; **Yihan Liu, Guangchun Yao** and **Xiuli Long**, School of Materials and Metallurgy, Northeastern University, Box 117, Shenyang 110004, China; and **Zhongsheng Hua,** School of Metallurgy and Resources, Anhui University of Technology, Anhui, China. Contact e-mail: djzneu@yahoo.cn.

In this paper, to further improve the fracture toughness of $NiFe_2O_4$ composite ceramics as inert anodes in severe environments, $NiFe_2O_4$ composite ceramics toughened with ZrO_2 fiber were fabricated with a two-step sintering process. The microstructure and the mechanical properties of $NiFe_2O_4$ composite ceramic reinforced with ZrO_2 fiber (ZrO_{2f}) were investigated and discussed in detail. Meanwhile, the pyroconductivity of ZrO_2 fiber-reinforced $NiFe_2O_4$ composites that serve as inert anodes working in molten cryolite is also studied.

2. Experimental

Commercially available NiO powder (>99.98%, Guoyao Co. Ltd., PR China), Fe_2O_3 powder (>99.3%, Xincheng Co. Ltd., PR China) were used as the starting powders. Yttria (Y_2O_3; 6.66%, mole)-stabilized commercial ZrO_2 fiber with 3-8 μm in mean diameter and 200 μm in medium length was also employed for the preparation of the composite ceramic material.

Raw materials (NiO power and Fe_2O_3 powder) were ground in distilled water via a ball-milling process using polypropylene jars with yttria-stabilized zirconia balls for 24 h and then dried thoroughly. The molar ratio of NiO to Fe_2O_3 was 1.87:1 in the powder mixture. Then, the mixtures were ground with 4 vol.% polyvinyl alcohol (PVA) binder and cold pressed at 160 MPa into a cylinder (ϕ100 mm × 20 mm) using a stainless steel die. The green ceramic bodies were calcined at 1000 °C for 6 h in air to produce $NiFe_2O_4$ ceramic matrix. The calcined matrix products were crushed thoroughly and ball-mixed with different amounts of ZrO_{2f} (0-4 wt.%) using ethanol as the grinding media. The properties of ZrO_{2f} adopted in this paper are listed in Table 1. After mixing for 24 h, the slurry was dried thoroughly in a vacuum oven. The resulting mixtures with 4 vol.% PVA binder were cold-pressed into rectangular bars (70 mm × 15 mm × 8 mm) using a stainless steel die under a uniaxial load of 200 MPa for 5 min. The bars were sintered at 1300 °C for 6 h in air atmosphere with a heating rate of 10 °C/min to produce ZrO_{2f}-reinforced $NiFe_2O_4$ composite ceramics and then cooled down to ambient temperature.

The microstructural features of sintered composites were observed using scanning electron microscope (SEM) (SSX-550, Japan) with simultaneous chemical analysis by energy-dispersive spectroscopy (EDS; EDAX Inc.). The phase composition was determined by a D/max 2RB x-ray diffraction (XRD, Japan) with Cu Kα radiation, pip voltage 40 kV, and current 100 mA. The bulk density of the specimens was measured by the Archimedes method. Bending strength was tested by three-point bending method on 70 mm × 15 mm × 8 mm bars, using a 30-mm span and a crosshead speed of 0.5 mm/min. The edges of all the specimens were chamfered to minimize the effect of stress concentration due to machining flaws. Fracture toughness (K_{IC}) was evaluated by a single-edge notched beam test with a 30-mm span and a crosshead speed of 0.05 mm/min using 70 mm × 15 mm × 8 mm bars, on the same jig used for the flexural strength measurements. All flexural and fracture bars were cut with tensile surface perpendicular to the cold-pressed direction. A minimum number of five specimens were tested for each experimental condition.

Table 1 Properties of ZrO_2 fibers adopted in this paper

Density, g/cm^3	Diameter, μm	Strength, GPa	Modulus, GPa	Melting point, °C	Thermal expansivity,/°C
4.45	3-8	2.1	340	2677	13×10^{-6}

The electrical pyroconductivity of solid materials was generally measured using a special device, which was generally combined with a heating furnace and based on the standard principles of DC two-point, four-point, or four-electrode technique (Ref 10, 20). Because of the difficulties in obtaining a good electrical contact at both ends of the specimen with the two-point technique, the four-point or four-electrode technique was adopted to determine the electrical pyroconductivity of $NiFe_2O_4$ composite ceramics, using the measuring apparatus as described in detail by Lai et al. (Ref 21).

The electrical conductivity σ is determined by the following equation (Ref 22):

$$\sigma = IL/US \quad \text{(Eq 1)}$$

where σ is the conductivity; I is the current intensity through the tested sample; L and U are the interval and voltage drop between two electrodes, respectively; and S is cross section of tested sample.

The measurements of conductivity for $NiFe_2O_4$ composites were carried out at temperatures ranging from 600 °C to 1000 °C with a temperature interval of 50 °C.

3. Results and Discussion

3.1 Microstructure and Phase Identification

The green cold-pressed NiO-Fe_2O_3-ZrO_{2f} ceramic billets with bulk densities of ~3.13 g/cm^3 were used to produce ZrO_{2f}-reinforced $NiFe_2O_4$ composite ceramics. The fracture surface of ZrO_{2f}-reinforced ceramic samples sintered at 1300 °C for 6 h is shown in Fig. 1.

It can be seen that when the ZrO_{2f} content is lower, the dispersion of fibers is more uniform. There is no obvious occurrence of agglomeration phenomena for ZrO_{2f} in the ceramic matrix, such as in the cases of 1 and 2 wt.%, as shown in Fig. 1(a) and (b), respectively. For 3 wt.% ZrO_{2f}-reinforced ceramic samples, ZrO_2 fibers were distributed uniformly at the ceramic matrix. Trajectories of many holes for fiber pull-out can be seen (Fig. 1c), which was confirmed by SEM. When 4 wt.% ZrO_{2f} was adopted in the ceramic matrix, obvious agglomeration and uneven distribution for ZrO_{2f} can be observed. It is the immediate cause of increase in porosity of sintered samples (Fig. 1d). In order to observe more clearly the interface between ZrO_{2f} and ceramic matrix, a larger magnification SEM image of polished surface from 3 wt.% ZrO_{2f}-reinforced $NiFe_2O_4$ composites is illustrated, in Fig. 1(e). It can be seen that ZrO_2 fiber is bonded tightly to $NiFe_2O_4$ composite ceramic matrix.

In order to further identify the phase transformation in the sintered samples, XRD patterns of ZrO_2 fibers adopted in this study and the synthesized $NiFe_2O_4$ composite ceramics with 3 wt.% ZrO_{2f} were also detected, and the detection results are shown in Fig. 2 and 3, respectively.

Besides Y_2O_3, only Y_2O_3-stabilized tetragonal zirconia polycrystals (Y-TZP) were observed for the ZrO_2 fibers adopted in this study. The XRD detection results for the polished surface of 3 wt.% ZrO_{2f}-reinforced ceramics, sintered at 1200, 1250, 1300, 1350, and 1400 °C for 6 h, are shown in Fig. 3. Besides the synthesized $NiFe_2O_4$ and excessive NiO in matrix, only the tetragonal phases for ZrO_2 are present. No phase transformation

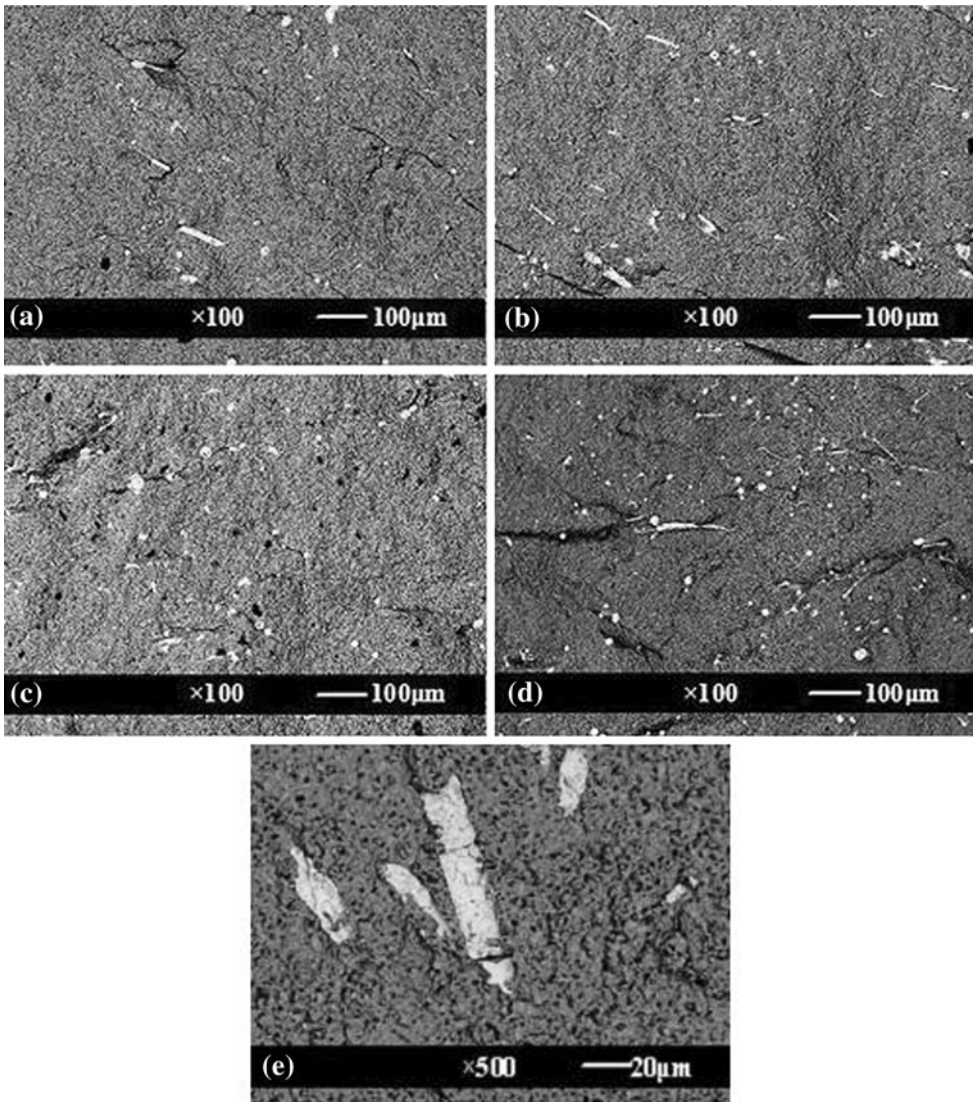

Fig. 1 SEM images of $NiFe_2O_4$ composites with different amounts of ZrO_2 fibers: (a) 1 wt.%; (b) 2 wt.%; (c) 3 wt.%; (d) 4 wt.%; and (e) higher magnification SEM image of polished surface from 3 wt.% ZrO_{2f}-reinforced $NiFe_2O_4$ composites

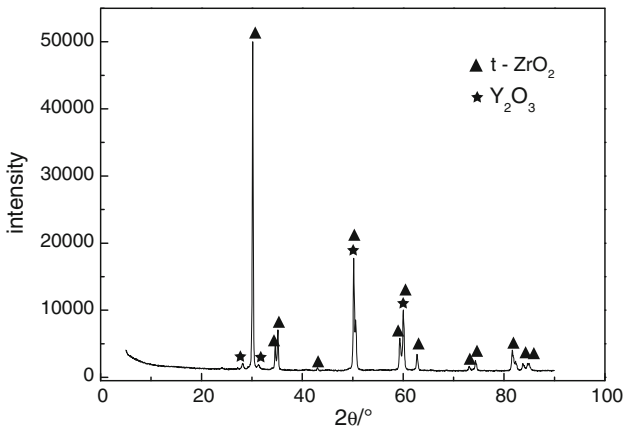

Fig. 2 XRD analysis of ZrO_2 fibers

for ZrO_2 fibers occurred during the sintering process with different temperatures. It is demonstrated that well-stabilized ZrO_2 fibers are obtained by Y_2O_3 (6.66%, mole) here.

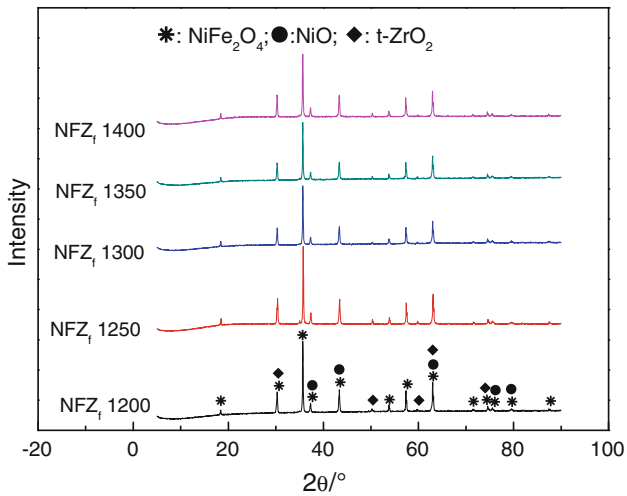

Fig. 3 XRD patterns of 3 wt.% ZrO_{2f}-reinforced $NiFe_2O_4$ composites with different sintering temperatures

3.2 Mechanical Properties

Results of the density and mechanical properties for NiO-Fe_2O_3-ZrO_{2f} ceramics sintered at 1300 °C for 6 h are listed in Table 2. It can be seen from Table 2 that the volume density decreases with increasing ZrO_{2f} content from the overall perspective. For all the samples sintered under the same condition, there is no difference in sintering driving force of NiO-Fe_2O_3-ZrO_{2f} system. Increasing ZrO_{2f} content would induce a higher average shear stress to the sintered ceramic matrix, which would result in a decrease in the sintering velocity. Simultaneously, it is difficult to make ZrO_{2f} disperse uniformly in the matrix. It is relatively easier for ZrO_{2f} to form three-dimensional rigid network skeleton producing bridges and springbacks among ZrO_2 fibers, which leads to structural defects and lower volume densities of sintered samples (Ref 14).

Bending strength increases obviously with ZrO_{2f} content increasing from 0 to 3 wt.%, but above 3.0 wt.%, a small change in value has been observed. For example, the bending strength increases from ~67.1 MPa for undoped samples to ~85.8 MPa for 3 wt.% ZrO_{2f}-doped samples. The variation trend of bending strength versus ZrO_{2f} content in this study is different from that of ZrO_{2f}-reinforced ZrB_2-SiC ceramics (Ref 23). It may be attributed to the different sintering temperatures of $NiFe_2O_4$ composites compared with ZrB_2-SiC-ZrO_{2f} system.

Generally speaking, for fiber or whisker-reinforced composites, in an optimal situation with fiber in a unidirectional arrangement, the strength σ can be represented by the following equation:

$$\sigma = \sigma_m V_m + \sigma_f V_f \quad \text{(Eq 2)}$$

where σ_m is matrix strength, V_m is the volume fraction of matrix, σ_f is fiber strength, and V_f is the volume fraction of fiber. There is a critical fiber volume fraction (P_c) to form rigid network skeletons in matrix (Ref 24). When $V_f < P_c$, σ will increase with increasing fiber content for the domination of fiber reinforcement on ceramic matrix; when $V_f \geq P_c$, σ is dependent on the densification of composites. In this paper, the variation trend of bending strength versus ZrO_{2f} content is in accordance with Ref 24.

It can obviously be seen from Table 2 that the fracture toughness was influenced by ZrO_{2f} content. With increasing ZrO_{2f} content from 0 to 3 wt.%, the fracture toughness increased from ~2.57 MPa $m^{1/2}$ to the maximum value of ~4.67 MPa $m^{1/2}$. Upon increasing the ZrO_{2f} content to 4 wt.%, the fracture toughness attains a value of 4.38 MPa $m^{1/2}$, which is lower than that obtained with 3 wt.% ZrO_{2f}-reinforced $NiFe_2O_4$ composites. There is a decreasing trend in the fracture toughness for ZrO_{2f}-reinforced $NiFe_2O_4$ composites when ZrO_{2f} content is increased from 3 to 4 wt.%. The possible reason is that fiber agglomeration occurred in the ceramic matrix with 4 wt.% ZrO_2 fiber, which might lead to structural defects in the composites. The fracture toughness was decreased when the ceramic composite was subjected to an external load. It is demonstrated that an optimal level of ZrO_2 fiber is of advantage to fracture toughness of $NiFe_2O_4$ composites, i.e., 3 wt.% ZrO_2 fiber in this case.

Table 2 Density and mechanical properties of NiO-Fe_2O_3-ZrO_{2f} ceramics

Specimen number	ZrO_{2f} content, wt.%	Density, g/cm^3	Bending strength, MPa	Fracture toughness, MPa $m^{1/2}$
1#	0	4.657	67.1 ± 1.5	2.57 ± 0.5
2#	1	4.635	79.2 ± 1.3	3.75 ± 0.3
3#	2	4.619	85.8 ± 1.2	4.36 ± 0.4
4#	3	4.598	89.0 ± 1.1	4.67 ± 0.3
5#	4	4.562	82.7 ± 1.6	4.38 ± 0.6

The effective toughening mechanisms of ZrO_2 fibers in composite ceramics including fiber debonding, fiber pull-out, crack deflection, crack bridging, and phase transformation were identified (Ref 23, 25-27). According to the results from XRD patterns from Fig. 2 and 3, it can be concluded that the phase transformation for ZrO_2 fibers to reinforce the ceramic matrix did not happen here. ZrO_2 fibers always remain tetragonal phases during sintering process here. SEM images of the fractured surface of 3 wt.% ZrO_{2f}-reinforced $NiFe_2O_4$ composites are shown in Fig. 4. A uniform distribution of short ZrO_2 fibers in $NiFe_2O_4$ matrix can be seen in Fig. 4(a). Figure 4(b) is a sketch of partial enlargement, which is marked as B in Fig. 4(a). According to Ref 27, in most cases, the crack propagates straight through the fibers with little deflection because of the low fracture strength of the fibers. However, on the fractured surface of the $NiFe_2O_4$ ceramics, some short fibers' debonding and no cracks propagating straight through the fibers were observed, as shown in Fig. 4(b). Because of the debonding at the fiber/matrix interface, the matrix crack did not penetrate the fibers, which then remained to bridge the matrix crack and restrained the crack from propagating (Ref 28). Addition of ZrO_2 fibers is beneficial for the enhancement of the fracture toughness of the $NiFe_2O_4$ ceramics.

Fibers' pull-out and rough fracture surfaces of the ceramics were also detected, as shown in Fig. 4(c). It can be seen from Fig. 4(d) that a perfect interface between ZrO_2 fiber and the matrix was observed, which also indicated that there was no obvious reaction between $NiFe_2O_4$ ceramics and ZrO_2 fibers. It is in accordance with the XRD results from Fig. 3. The enhancement in the mechanical properties of the ceramic matrix, which is provided by perfect interface between ZrO_2 fibers and the synthesized $NiFe_2O_4$, is similar to that observed in ZrB_2-SiC composites (Ref 29).

The analysis from Fig. 4 indicated that the crack acquired not only the propagating resistance of matrix but also the interfacial shear resistance to cause the fibers pull-out and debonding. At the same time, the rough fracture surface of the ceramics (Fig. 4d) implied that crack deflection might be another toughening mechanism because the crack swerving and twisting along fiber/matrix interface would expend more energy than that expended by crack propagating straight (Ref 30). Thus, the extensive crack interactions among the short fibers during fracturing process increased the fracture surface energy and thus contributed to the improvement in the toughness, marked as the region A in Fig. 4(a).

3.3 Pyroconductivity

Besides the analysis of reinforcement for ZrO_2 fiber on the mechanical properties of $NiFe_2O_4$ composites, the pyroconductivity of ZrO_{2f}-reinforced $NiFe_2O_4$ as inert anodes was also studied. Arrhenius equation for the conductivity of normal semiconductors, like $NiFe_2O_4$, was suggested as follows (Ref 31):

$$\rho_{DC} = \rho_0 \exp\left(\frac{E}{kT}\right) \quad \text{(Eq 3)}$$

where ρ_{DC} is DC electrical resistivity; E is the activation energy in electron volts (eV), which is needed to release an

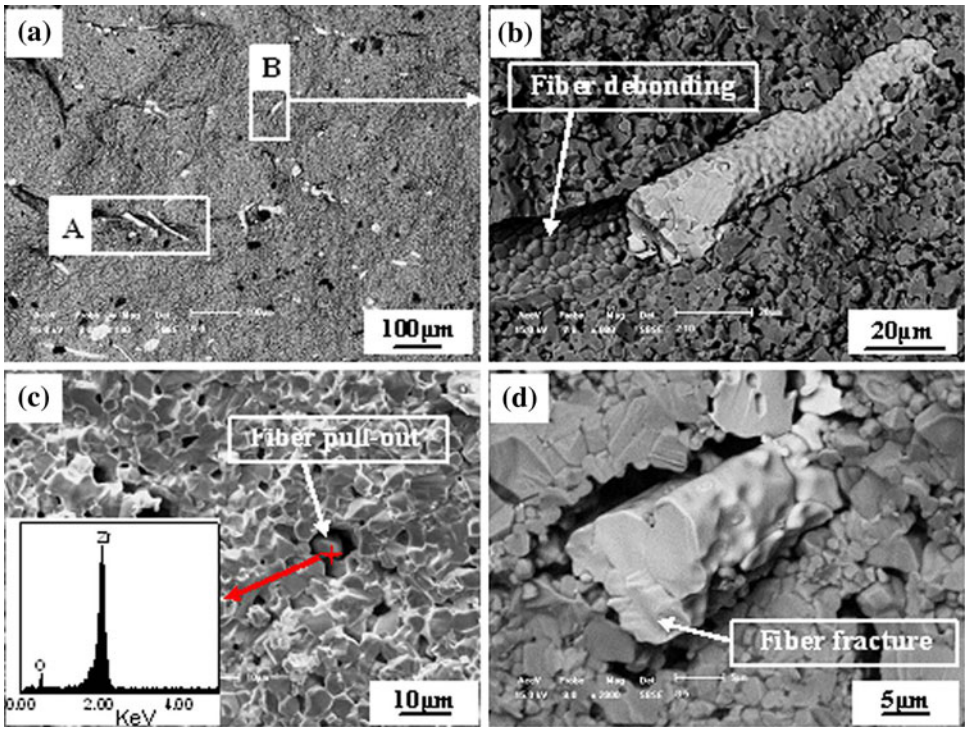

Fig. 4 SEM images of the fractured surface of 3 wt.% ZrO_{2f}-reinforced $NiFe_2O_4$ composites at different magnifications

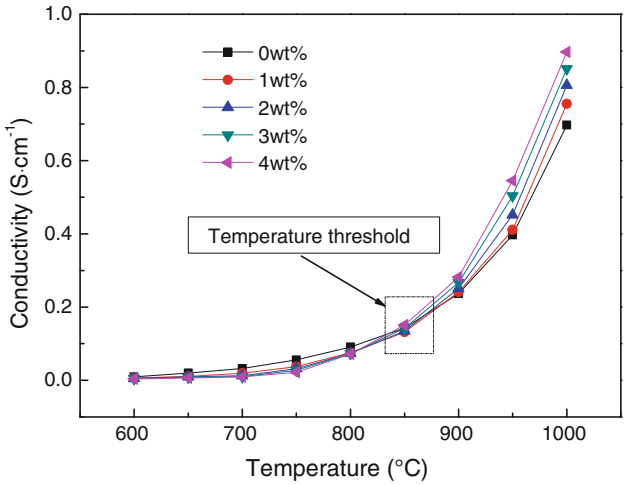

Fig. 5 The conductivity vs. temperature of ZrO_{2f}-reinforced $NiFe_2O_4$ composites

electron from one ion to the neighboring one giving rise to the electrical conductivity (Ref 32); k is the Boltzmann's constant; and T is the absolute temperature. Conductivity value of σ is the inverse of ρ_{DC}. The conductivity versus temperature curve of the ZrO_{2f}-reinforced $NiFe_2O_4$ composites is shown in Fig. 5. The same temperature interval of 50 °C was applied to study the conductivity of each ZrO_{2f}-reinforced $NiFe_2O_4$ sample at temperatures ranging from 600 to 1000 °C.

From Fig. 5, the conductive behavior is observed when the temperature is greater than 600 °C. Also, conductivity increases with increasing temperature up to 850 °C, a threshold marked as a small square in Fig. 5. In the range from 600 to 850 °C, the conductivity of the undoped samples is greater than that of the ZrO_{2f}-reinforced $NiFe_2O_4$ samples. However, it is interesting to note that the conductivity of the ZrO_{2f}-reinforced samples is much better than that of the undoped samples when the temperature is greater than 850 °C. The more the content of ZrO_2 fiber that was introduced into the ceramic matrix, the higher the value of conductivity that could be obtained. When temperature reaches up to 950 °C, the conductivity value of the samples reinforced with 4 wt.% ZrO_2 fibers reaches 0.63 S/cm, which shows an increment of 37.8% compared with 0.45 S/cm obtained for the undoped samples.

However, nearly no conductive behavior for ZrO_2 fiber is obviously observed at low temperature, as the introduction of ZrO_2 fiber into the ceramic matrix decreased the conductivity of the composites. It can be concluded that the conductivity of ceramic composites is dependent on $NiFe_2O_4$ matrix. Also with increasing ZrO_{2f} content, a higher porosity will be induced in the matrix, which is a barrier for good interaction among conductive phases. It is detrimental to the improvement of conductivity. However, ZrO_{2f}-reinforced $NiFe_2O_4$ obtains better conductivity at higher temperature (>850 °C). This phenomenon is probably attributed to the admittance of partial Zr^{4+} ions into the lattice of $NiFe_2O_4$, which will substitute partial Fe^{3+} ions to form a solid solution. It can lead to lattice transformation of $NiFe_2O_4$. This transformation could be confirmed by the differences in the values of the lattice parameters a, b, and c: 0.83370, 0.83370, 0.83370 nm for the undoped and 0.83379, 0.83379, 0.83379 nm, for the 3 wt.% ZrO_{2f}-reinforced ceramic samples, respectively. Hence, the substitution may produce quasi-free electrons as follows (Ref 33):

$$3ZrO_2 \xrightarrow{NiFe_2O_4} 3Zr'_{Fe} + 6O_O^X + V'''_{Fe} \quad \text{(Eq 4)}$$

where Zr'_{Fe} represents the occupancy of Fe^{3+} ions by Zr^{4+} ions, O_O^X means the oxygen ions at normal lattice point, and

V'''_{Fe} represents the cation vacancy. The substitution effect of partial Zr^{4+} ions to produce quasi-free electrons for the enhancement of electrical conductivity is limited by the concentration of conductive ions produced in this way.

There is another conductive mechanism—oxygen ionic conduction in ZrO_{2f} for improving the conductivity of the ceramic matrix. For the Y_2O_3-stabilized ZrO_{2f}, Y^{3+} ions occupied the sites of Zr^{4+} ions after the addition of Y_2O_3 to ZrO_{2f}, as shown by the following equation (Ref 34):

$$Y_2O_3 \xrightarrow{ZrO_2} 2Y'_{Zr} + V_{\ddot{O}} + 3O \quad \text{(Eq 5)}$$

In the crystal lattice with a couple of Y^{3+} substitutions, an oxygen vacancy could be produced. Zr-O spacing is 0.211 nm, which is 0.017 nm smaller than that of Y-O, and so anionic vacancy is close to Zr^{4+}. Vacancy distribution around Zr^{4+} in ZrO_2 crystal lattice will decrease the partial repelling force of O-O and result in coordination sphere distortion, which is beneficial to filling the lattice defects of ZrO_2 (Ref 35). Consequently, the crystal transformation of ZrO_2 could be avoided, and the Y_2O_3-stabilized ZrO_2 can remain as tetragonal phase during the sintering process. Also, the ionic conductance (σ_i) of the Y_2O_3-stabilized tetragonal ZrO_2 is strongly dependent on crystal structure and temperature. Ionic conductance (σ_i) of tetragonal ZrO_2 is much higher than that of monoclinic and cubic phases, and σ_i increased exponentially with the increasing temperature (Ref 36). Hence, when electrolyte temperature is increased up to 1000 °C, the conductivity of $ZrO_{2(f)}/NiFe_2O_4$ composites is increase to much higher than that of $NiFe_2O_4$ samples.

4. Conclusions

In the present study, ZrO_{2f}-NiO-Fe_2O_3 composites were prepared through a two-step sintering process. XRD of the prepared samples shows that $NiFe_2O_4$, NiO, and ZrO_2 phases are the main phases present in the sintered ceramic matrix. ZrO_2 fiber remains as tetragonal phase during the sintering process, and no phase transformation was detected. Among all the doping levels, there is a uniform distribution of short ZrO_2 fibers in 3 wt.% ZrO_{2f}-reinforced $NiFe_2O_4$ matrix. The volume density decreases with the increasing ZrO_{2f} content from the overall perspective. The values for both the bending strength and fracture strength of 3 wt.% ZrO_{2f}-reinforced $NiFe_2O_4$ samples reached their respective maximum values of ~89.0 MPa and ~4.67 MPa $m^{1/2}$. The observed toughening mechanisms were attributed to the fiber debonding, fiber bridging, crack deflection, and fiber pull-out toughening. The conductivity of ZrO_{2f}-reinforced $NiFe_2O_4$ is dependent on temperature and ZrO_{2f} content. When the electrolytic temperature is increased up to 950 °C, the conductivity value of the samples reinforced with 4 wt.% ZrO_2 fibers attains 0.63 S/cm, which shows an increment of 37.8% compared with 0.45 S/cm obtained for the undoped samples. The two main conductive mechanisms of ZrO_2 fiber in the matrix are the substitution of Fe^{3+} to produce quasi-free electrons and oxygen ionic conducting mechanism.

Acknowledgments

The authors gratefully acknowledge the financial support from the State Key Program of the National Natural Science of China (No. 50834001; No. 50971038) and the National High Technology Research and Development Program of China (863 Program) (No. 2009AA03Z502).

References

1. S.E. Shirsath, B.G. Toksha, and K.M. Jadhav, Structural and Magnetic Properties of In^{3+} Substituted $NiFe_2O_4$, *Mater. Chem. Phys.*, 2009, **117**, p 163–168
2. Y.M. Al Angari, Magnetic Properties of La-substituted $NiFe_2O_4$ via Egg-White Precursor Route, *J. Magn. Magn. Mater.*, 2011, **323**, p 1835–1839
3. A. Goldman, *Modern Ferrite Technology*, Marcel Dekker, New York, 1993
4. D.R. Patil and B.K. Chougule, Effect of Copper Substitution on Electrical and Magnetic Properties of $NiFe_2O_4$ Ferrite, *Mater. Chem. Phys.*, 2009, **117**, p 35–40
5. O.M. Hemeda, M.Z. Said, and M.M. Barakat, Spectral and Transport Phenomena in Ni Ferrite-substituted Gd_2O_3, *J. Magn. Magn. Mater.*, 2001, **224**, p 132–142
6. M.A. Gabal and Y.M. Al Angari, Effect of Diamagnetic Substitution on the Structural, Magnetic and Electrical Properties of $NiFe_2O_4$, *Mater. Chem. Phys.*, 2009, **115**, p 578–584
7. R.S. Devan, Y.D. Kolekar, and B.K. Chougule, Effect of Cobalt Substitution on the Properties of Nickel-Copper Ferrite, *J. Phys.: Condens. Matter.*, 2006, **18**, p 9809–9821
8. X.H. Cao, J.H. Meng, F. Mi, Z.H. Zhang, and J. Sun, Preparation and Magnetic Property Investigation of a Nickel Spinel Ferrite-Coated Tetrapod-Like ZnO Composite, *Solid State Commun.*, 2011, **151**(9), p 678–682
9. S.P. Ray, *Inert Anodes for Hall Cells*, TMS, Warrendale, PA, 1986, p 287–298
10. E. Olsen and J. Thonstad, Nickel Ferrite as Inert Anodes in Aluminium Electrolysis (Part I): Material Fabrication and Preliminary Testing, *J. Appl. Electrochem.*, 1999, **29**, p 293–299
11. D.R. Sadoway, Inert Anodes for the Hall Hároult Cell: The Ultimate Materials Challenge, *JOM*, 2001, **53**, p 34–35
12. L.J. Berchmans, R.K. Selvan, and C.O. Augustin, Evaluation of Mg^{2+}-substituted $NiFe_2O_4$ as a Green Anode Material, *Mater. Lett.*, 2004, **58**, p 1928–1933
13. S.T. Zhang, G.C. Yao, and Y.H. Liu, Study on Sintering Technique of $NiFe_2O_4/SiC_w$ Used as Matrix of Inert Anodes, *J. Funct. Mater.*, 2005, **4**(36), p 569–571 (in Chinese)
14. S.J. Guo, *Powder Sintering Theory*, Metallurgical Industry Press, Beijing, 1998, p 201–238
15. D. Gómez-García, J. Martínez-Fernández, A. Domínguez-Rodríguez, P. Eveno, and J. Castaing, Deformation Mechanisms for High-Temperature Creep of High Yttria Content Stabilized Zirconia Single Crystals, *Acta Mater.*, 1996, **44**(3), p 991–999
16. J. Lin, X.H. Zhang, Z. Wang, and W.B. Han, Microstructure and Mechanical Properties of ZrB_2-SiC-ZrO_{2f} Ceramic, *Scr. Mater.*, 2011, **64**, p 872–875
17. H. Miyazaki, Y. Yoshizawa, and K. Hirao, Effect of the Volume Ratio of Zirconia and Alumina on the Mechanical Properties of Fibrous Zirconia/Alumina Bi-phase Composites Prepared by Co-extrusion, *J. Eur. Ceram. Soc.*, 2006, **26**, p 3539–3546
18. B. Budiansky and Y.L. Cui, Toughening of Ceramics by Short Aligned Fibers, *Mech. Mater.*, 1995, **21**, p 139–146
19. J.P. Singh, D. Singh, and M. Sutaria, Ceramic Composites: Roles of Fiber and Interface, *Compos. A*, 1999, **30**, p 445–450
20. S. Pietrzyk and R. Oblakowski, *Electrical Conductivity of Cryolite Electrolytes During the Liquid-Solid Phase Transition*, TMS, Warrendale, PA, 2002, p 405–414
21. Y.Q. Lai, J. Li, Z.L. Tian, G. Zhang, and Y.X. Liu, *An Improved Pyroconductivity Test of Spinel-containing Cermet Inert Anodes in Aluminum Electrolysis Cells*, A. T. Tabereaux, TMS, Warrendale, PA, 2004, p 339–344
22. Y.Q. Lai, Z.L. Tian, J. Li, S.L. Ye, and Y.X. Liu, Preliminary Testing of $NiFe_2O_4$-NiO-Ni Cermet as Inert Anode in Na_3AlF_6-AlF_3 Melts, *Trans. Nonferrous Met. Soc. China*, 2006, **16**, p 654–658
23. J. Lin, X.H. Zhang, Z. Wang, W.B. Han, and H. Jin, Microstructure and Mechanical Properties of Hot-Pressed ZrB_2-SiC-ZrO_{2f} Ceramics with Different Sintering Temperatures, *Mater. Des.*, 2012, **34**, p 853–856

24. A.H. Elizabeth and J.C. Michael, Two-Dimensional Whisker Percolation in Ceramic Matrix-Ceramic Whisker Composites, *J. Am. Ceram. Soc.*, 1989, **72**(2), p 303–305
25. L. Silvestroni, D. Sciti, C. Melandri, and S. Guicciardi, Toughened ZrB_2-based Ceramics Through SiC Whisker or SiC Chopped Fiber Additions, *J. Eur. Ceram. Soc.*, 2010, **30**, p 2155–2164
26. A.L. Chamberlain, W.G. Fahrenholtz, G.E. Hilmas, and D.T. Ellerby, High-Strength Zirconium Diboride-Based Ceramics, *J. Am. Ceram. Soc.*, 2004, **87**, p 1170–1172
27. D. Sciti, S. Guicciardi, and L. Silvestroni, SiC Chopped Fibers Reinforced ZrB_2: Effect of the Sintering Aid, *Scr. Mater.*, 2011, **64**, p 769–772
28. G.H. Zhou, S.W. Wang, J.K. Guo, and Z. Zhang, The Preparation and Mechanical Properties of the Unidirectional Carbon Fiber Reinforced Zirconia Composite, *J. Eur. Ceram. Soc.*, 2008, **28**, p 787–792
29. W.G. Fahrenholtz, G.E. Hilmas, I.G. Talmy, and J.A. Zayko-ski, Refractory Diborides of Zirconium and Hafnium, *J. Am. Ceram. Soc.*, 2007, **90**(5), p 1347–1364
30. F.Y. Yang, X.H. Zhang, J.C. Han, and S.Y. Du, Mechanical Properties of Short Carbon Fiber Reinforced ZrB_2-SiC Ceramic Matrix Composites, *Mater. Lett.*, 2008, **62**, p 2925–2927
31. A.I. El Shora, M.A. El Hiti, M.K. El Nimr, M.A. Ahmed, and A.M. El Hasab, Semiconductivity in $Ni_{1+x}Mn_xFe_{2-2x}O_4$ Ferrites, *J. Magn. Magn. Mater.*, 1999, **204**, p 20–28
32. J. Smit and H.J.P. Wijn, *Ferrites*, Cleaver-Hume Press, London, 1959
33. Y.S. Yin and J. Li, *Zirconia Ceramics and Composite Materials*, Chemical Industry Press, Beijing, 2004
34. C.F. Wang, G.X. Li, and S.L. Qu, Effect of Adding Y_2O_3 in Ceramic Electrodes on the Electrical Conductivities, *Rare Met.*, 1992, **11**(4), p 255–259
35. A. Pierre and P.T. Jean, Structure and Iron Mobility of Zirconia at High Temperature, *J. Am. Ceram. Soc.*, 1985, **68**(1), p 34–40
36. F. Boulch and E. Djurado, Structural Changes of Rare-Earth-Doped, Nanostructured Zirconia Solid Solution, *Solid State Ion.*, 2003, **157**(1–4), p 335–340